CRYSTAL GROWTH & DESIGN

pubs.acs.org/crystal

Article

Crystal Structure of Ritonavir Form IV and Thermodynamic Relationships between Ritonavir Polymorphs

Stephan D. Parent, Jared P. Smit,* Dale K. Purcell, Pamela A. Smith, Pierre Le Maguerès, Haley C. Bauser, and Adrian Radocea

Cite This: *Cryst. Growth Des.* 2026, 26, 1386−1392

Read Online

ACCESS | Metrics & More | Article Recommendations | Supporting Information

ABSTRACT: The crystal structure of Ritonavir Form IV is reported. The structure was determined by electron diffraction, and the molecular conformation and hydrogen bonding show similarities to those of Forms I and III. Form II is shown to be the most thermodynamically stable of the four known polymorphs.

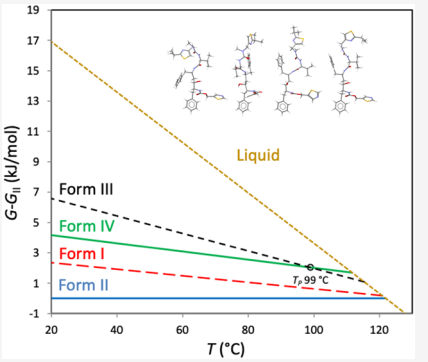

INTRODUCTION

Polymorphism is the ability of a solid material to exist in more than one crystal form, with each polymorph possessing a distinct crystal structure with distinct physical properties.[1] The crystalline form of an active pharmaceutical ingredient (API) can impact the drug's formulation, release, and storage stability.[2−4] Determining the relative stability of an API's polymorphs as well as the transition behavior between the forms is a critical step in the development of the drug product.[5] Phase transitions between polymorphs can be thermodynamically reversible or irreversible. Polymorphs that undergo reversible transformations at a specific phase transition temperature (T_p) are termed enantiotropic. Conversely, forms that transform irreversibly are monotropic.[6] The Burger and Ramberger Heat of Fusion Rule provides a thermodynamic criterion for distinguishing between these two relationships: if the polymorph with the higher melting temperature has a lower heat of fusion, the two forms are enantiotropic; otherwise, they are monotropic.[7,8] This principle is grounded in the relationships among Gibbs free energy, enthalpy, and entropy.

The polymorphic landscape of the antiviral protease inhibitor Ritonavir (RTV) has long served as an example of the importance of understanding the thermodynamic relationships between polymorphs. Developed and marketed as Norvir for the treatment of human immunodeficiency virus (HIV) using the only known polymorph (Form I) at the time, the product had to be recalled and reformulated after the appearance of the more stable and less soluble Form II polymorph led to difficulties in producing Form I.[9,10] The crystal structures for Form I and Form II have since been determined.[11] Decades after the recall crisis, RTV is still used in products such as Paxlovid, and another anhydrous polymorph, Form III, was reported, its crystal structure was determined, and relationships to Forms I and II were investigated.[12−14] A fourth anhydrous polymorph has also been observed.[15] Herein, we report the crystal structure of the anhydrous polymorph Form IV, synthesized through the desolvation of a dichloromethane solvate and determined through electron diffraction methods, and the relative thermodynamic relationships between the known polymorphs.

EXPERIMENTAL SECTION

Materials

RTV lot GLST20230817 was obtained from Parchem (New Rochelle, NY) and was used without further purification.

Preparation of Form IV: Powder samples of the previously reported bis(DCM) solvate were obtained from undersaturated solutions of RTV in DCM, with concentrations around 16 g L^{-1}, by adding five volumes of hexane.[15] Oiling out was evident as the solution transitioned from clear to turbid. The emulsion was left undisturbed for 1 day, allowing crystallization into thin, wispy needles. Once solids are isolated from the suspension and exposed to air, the solvent is

Received: November 5, 2025
Revised: January 15, 2026
Accepted: January 16, 2026
Published: January 23, 2026

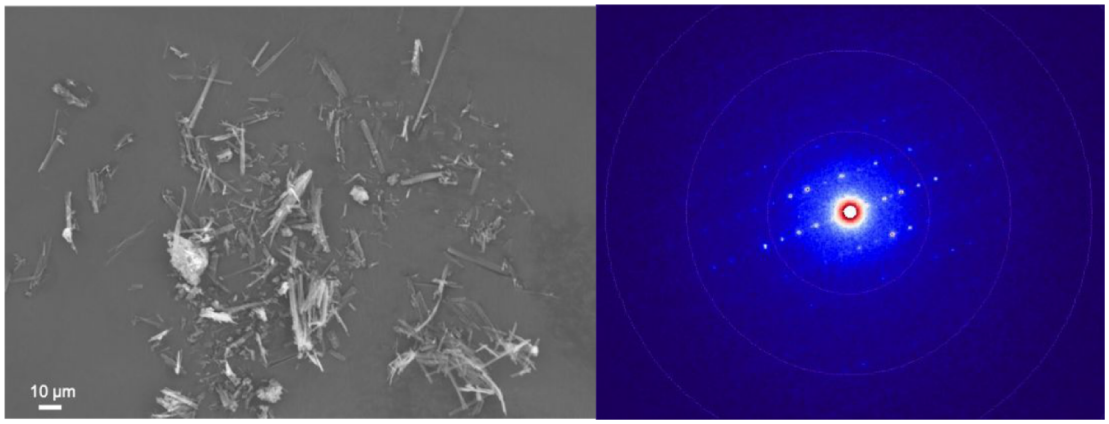

Figure 1. Crystallites of Ritonavir Form IV and an electron diffraction image.

quickly lost from the bis (DCM) solvate and conversion to the metastable anhydrate RTV Form IV was observed. The resulting crystallites are shown in Figure 1 and were too small for traditional single-crystal XRD; therefore, electron diffraction methods were utilized.

Preparation of Form III: 1 g of RTV Form II was dispensed onto a glass slide and heated in an oven to 130 °C until the sample was a clear liquid after 30 min. The sample was then transferred to an oven at 83 °C for 1 day, after which solids were recovered from the melt.

Preparation of Form II: 10.23 g of RTV was dissolved in 30 mL of ethanol and refrigerated overnight, vacuum filtered, and stored in an open jar under ambient conditions for 10 days.

Preparation of Form I: 5.57 g of RTV was heated and dissolved in 165 mL of ethyl acetate. The solution was cooled overnight to room temperature, filtered, and then left to evaporate until the solution volume was reduced to approximately half. 400 mL of hexane was added to induce precipitation.

Electron Diffraction Crystal Structure Determination

MicroED measurements were performed using a Rigaku XtaLAB Synergy-ED equipped with a JEOL 200 kV electron source, column, and beam optics and a Rigaku HyPix-ED detector, all optimized for operation in the microED experimental setup.[16] The electron beam has a wavelength of 0.0251 Å and runs in a high vacuum of about 1.5×10^{-7} Torr. The sample was prepared by dropping a 3 mm Cu TEM grid with a continuous carbon film into the powder to gather crystallites. The grid was held using a pair of inverted tweezers, which were tapped on their side to shed some of the powder and obtain a grid with sparsely spread crystallites. The grid was then placed into a Gatan Elsa sample cryo-holder Model 698, and the sample was cooled down to 100 K, using a Gatan transfer station. Finally, the cryo-holder was inserted into the XtaLAB Synergy-ED.

Several crystallites of Form IV were screened for diffraction using the Rigaku program CrysAlisPro-ED. The best diffracting crystallites were thin plates, with a width of a micrometer or less. However, the sample showed rapid decay when traversed by the electron beam, with diffraction disappearing within a minute or two. Therefore, crystallites were screened and centered using the "Flash mode" feature in CrysAlisPro-ED, which opens the beam only when images are collected and blanks it otherwise. Data were collected rapidly and concurrently processed using CrysAlisPro-ED. Given the low-symmetry space group, the completeness of individual data sets ranged between 46% and 64%, depending on the amount of rotation permitted per crystallite and their orientation on the grid. Therefore, four data sets were merged to 0.80 Å resolution, yielding 100% completeness and 3.3 redundancy, an overall $I/\sigma(I)$ of 5 and R_{int} of 16%. Statistics on both the individual and the merged data sets are shown in Tables S2 and S3 in Supporting Information, along with pictures of the crystallites used for data collection and examples of their electron diffraction patterns.

Using Olex2, the structure was readily solved with the ShelXT structure solution program in space group $P2_1$, using intrinsic phasing and kinematically refined with the ShelXL refinement package, using least-squares minimization.[17−19] All atoms were refined in an anisotropic approximation. The hydrogen atoms were placed in their idealized positions and refined as riding atoms. Hydrogen bond distances used for structure refinement from neutron diffraction data were used for final refinements in ShelXL (using the command "neutronhdist"), as hydrogen bond distances observed from electron diffraction are closer to those observed from neutron diffraction than from X-ray diffraction. There is one molecule per asymmetric unit. At one end of the molecule, the atoms in the 5-membered heterocycle and the isopropyl group branching out of it show enlarged thermal ellipsoids, indicative of a disorder. However, the data quality did not allow for modeling this disorder.

Crystal data for $C_{37}H_{48}N_6O_5S_2$ ($M = 720.96$ g/mol): monoclinic, space group $P2_1$ (no. 4), $a = 13.7334(17)$ Å, $b = 5.1212(5)$ Å, $c = 26.091(10)$ Å, $\beta = 98.205(19)$ °, $V = 1816.2(7)$ Å^3, $Z = 2$, $T = 100.3(2)$ K, $D_{calc} = 1.318$ g/cm,[3] F(000) = 303, 24883 reflections measured ($0.106° \leq 2\Theta \leq 1.798°$), 7447 unique ($R_{int} = 0.1645$) which were used in all calculations. The final R_1 was 0.1755 ($I > 2\sigma(I)$) and wR_2 was 0.4271. The crystal structure information can be found under the CCDC deposition number 2482055.

Scanning Electron Microscopy

Scanning electron microscopy (SEM) is performed using a HITACHI S-3400N variable pressure scanning electron microscope. Under high vacuum mode, an Everhart-Thornley (ETD) detector is used unless otherwise noted. Beam (accelerating) voltage is 5.0 to 20.0 kV, and the resolution of the image is 2560 × 1920 unless otherwise noted. Data are collected using HITACHI High-Tech Science Systems operating software version 1.20.

Gold Coating (Au) for SEM

The sample is sputter coated using a Cressington 108 Auto/SE Sputter Coater equipped with a Rotary-Planetary-Tilting stage at presets of 30 mA and 0.15 mbar (in Ultra-Pure Argon) for 55 s, while the sample is rotating at an approximate 40° angle.

Differential Scanning Calorimetry: Sample Preparation and Analysis

RTV polymorphs were analyzed by differential scanning calorimetry (DSC) using a TA Instruments Model 25. The instrument was calibrated with indium. Samples were weighed in an aluminum pan with a crimped lid. An empty aluminum pan was used as a reference. The samples were equilibrated at either 50 or 100 °C and heated to 150 °C at a rate of 1, 10, or 20 °C/min under a 50 cc/min nitrogen purge. A sigmoidal baseline was used for measuring the heat of fusion.

https://doi.org/10.1021/acs.cgd.5c01571
Cryst. Growth Des. 2026, 26, 1386−1392

Table 1. Space Groups, Unit Cell Parameters, and Derived Densities of Known RTV Forms

Form	I	II	III[a]	III[b]	IV
Space Group	$P2_1$	$P2_12_12_1$	$C2$	$P1$	$P2_1$
a (Å)	13.344(2)	9.831(6)	23.354(2)	9.9264(6)	13.7334(17)
b (Å)	5.2150(8)	18.485(11)	4.9531(4)	11.9512(7)	5.1212(5)
c (Å)	26.693(4)	20.261(12)	33.648(3)	34.007(2)	26.091(10)
α (°)	90	90	90	89.710(2)	90
β (°)	103.456(2)	90	91.342(10)	82.053(2)	98.205(19)
γ (°)	90	90	90	77.733(2)	90
Volume (Å^3)	1806.547	3681.951	3891.155	3903.128	1816.2
Density (g/cm^3)	1.325	1.301	1.231	1.227	1.318
Temperature (K)	100	100	100	100	100

[a]Original structure determination. [b]Structure redetermination.

Thermogravimetric Analysis: Sample Preparation and Analysis

A 4.517 mg sample of RTV Form IV was analyzed by thermogravimetric analysis (TGA) using a TA Instruments Model 55. The instrument was calibrated with nickel. The sample was placed into a platinum pan and heated from ambient temperature to 250 °C at a rate of 10 °C/min under a 40 cc/min nitrogen purge.

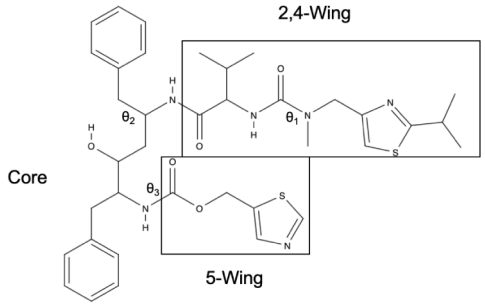

Figure 2. Molecular structure of Ritonavir with the wings, core, and relevant torsions labeled.

RESULTS AND DISCUSSION

The molecular orientations and hydrogen bond motifs of Forms I, II, and III have been compared previously using the wing and core description depicted in Figure 2.[13] Additionally, the primary torsion angles differentiating the polymorphs have been labeled θ_1 at the *N*-methyl urea group, θ_2 at the benzyl group, and θ_3 at the carbamate group, as also shown in Figure 2.[20] Both naming conventions are retained in this work.

Structural Comparisons

The unit cells of all known anhydrous forms are listed in Table 1 and the molecular conformations are shown in Figure 3.

The unit cell of Form IV is similar to that of Form I, and it follows that the molecular frameworks are also similar. The hydrogen bond donors and acceptors are identical between Forms I and IV, creating 1D hydrogen bond networks, as shown in Figure 4.

The 5-wing (θ_3) and half of the core have identical orientations as well. A core benzyl moiety at torsion θ_2 and the isopropyl thiazole moiety of the 2,4-wing at torsion θ_1 are rotated by approximately 180°, differentiating Form IV from Form I, as can be seen in Figures 4 and 5.

The hydrogen-bonded pairs are also identical in the molecular framework of Form III, and the molecular conformation and torsion angles of Form III are similar to those of Form IV, as shown in Figure 5. However, the slight difference in the conformation of the molecule places the hydroxyl − thiazole hydrogen bond in a position that creates a second dimension not present in the framework of Forms I or IV, as depicted in Figure 4. Form III contains the only two-

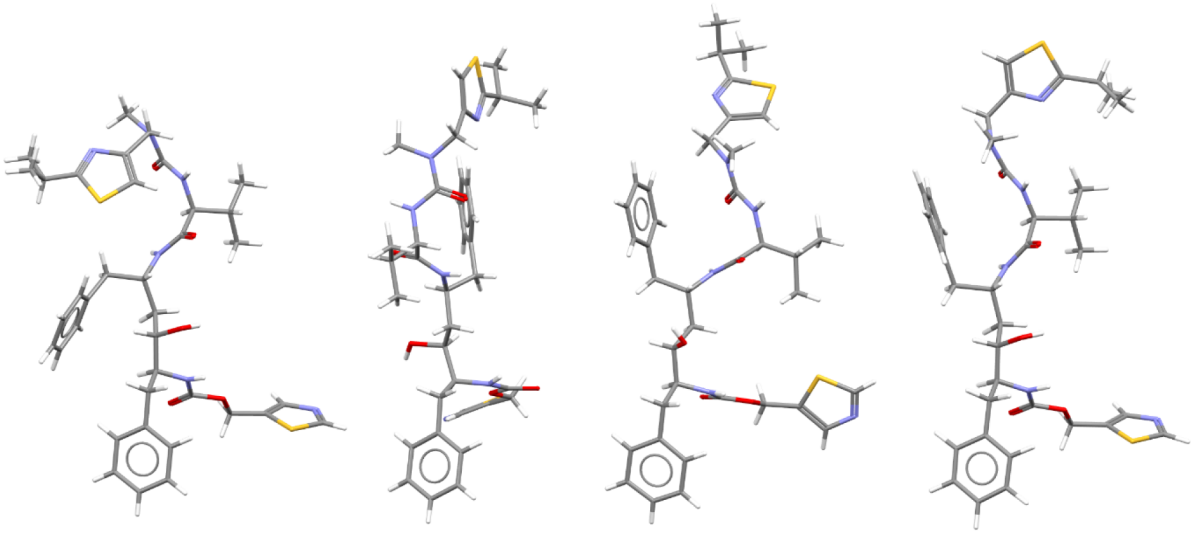

Figure 3. Molecular conformations of Forms I, II, III, and IV (left to right).

https://doi.org/10.1021/acs.cgd.5c01571
Cryst. Growth Des. 2026, 26, 1386−1392

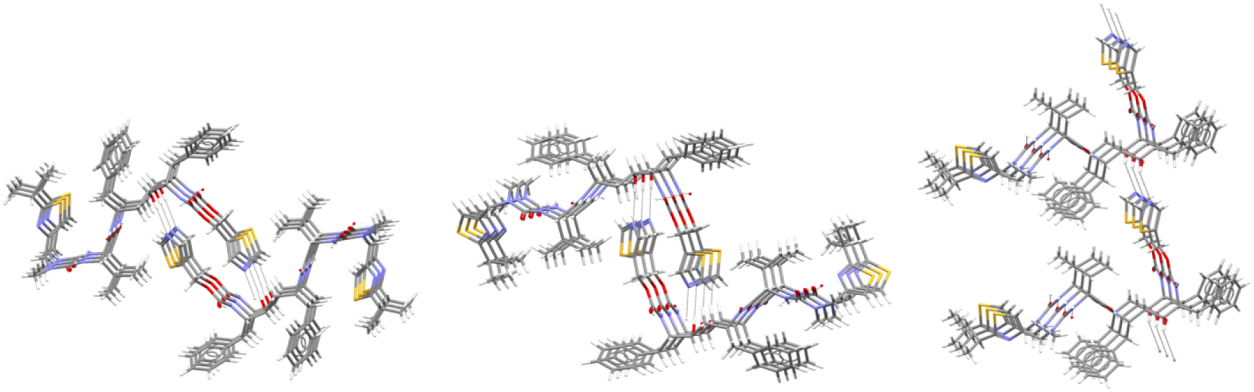

Figure 4. Hydrogen bonding in the frameworks of Forms I, IV, and III (left to right).

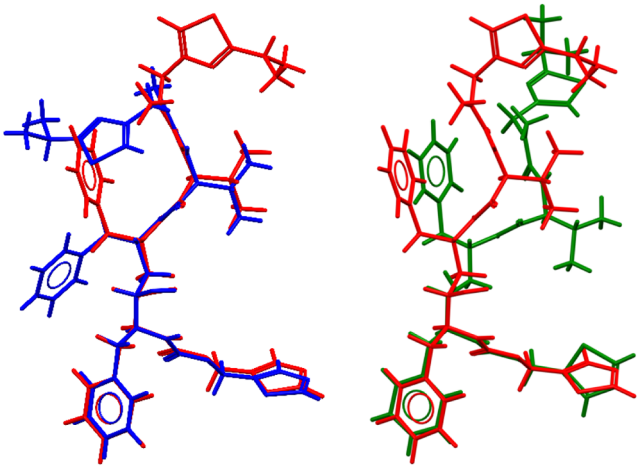

Figure 5. Overlay of the molecular conformation of Forms IV (red), I (blue), and III (green).

dimensional hydrogen-bond network of the four known polymorphs. Form III has since been redetermined with lower symmetry, containing four independent molecules in the asymmetric unit and, therefore, four molecular conformations rather than one disordered molecular conformation in the original structure determination.[23] However, the hydrogen-bonding conclusions remain unchanged. The hydrogen bonding in the framework of Form II is significantly different from that of the other three forms and likely contributes to the higher thermodynamic stability of Form II relative to the other three forms, despite being the third most dense polymorph (Table 1).

The different molecular conformations lead to the molecular packing arrangements shown in Figure 6. Forms I, III, and IV each display a crystallographic axis where the molecules are stacked in an identical orientation uninterrupted, resulting in similar weak aromatic intermolecular interactions between the forms. Form II does not have a comparable crystallographic axis as adjacent molecules are in different orientations in all directions, and therefore, Form II contains no intermolecular aromatic interactions.

Relative Thermodynamic Relationship Determination

The differential scanning calorimetry (DSC) and thermogravimetric analysis (TGA) plots for Form IV are shown in Figure 7 along with DSC thermograms of the four known anhydrous polymorphs at a rate of 10 °C/min. Form IV melts with an onset at 111.7 °C, termination of fusion at 117.4 °C, and enthalpy of 71.8 J/g, based on the averaged values obtained from 1, 10, and 20 °C/min DSC thermograms (vide infra). Form IV has the lowest melting point of the four known polymorphs.

The Heat of Fusion Rule was applied to the four known anhydrous polymorphs of RTV. Their melting onset temperatures (T_m) and heats of fusion (ΔH_f) were determined using DSC thermograms obtained at 1 °C/min, 10 °C/min, and 20 °C/min, as shown in Figure 8. Multiple ramp rates were employed to isolate and confirm the thermal event as true melting and to mitigate potential complications from concurrent or competitive solid-state processes.[21−23] Averaging the data from different ramp rates also helps to obtain a more accurate and robust value for the heat of fusion, which is a crucial thermodynamic parameter for applying the Heat of Fusion Rule.

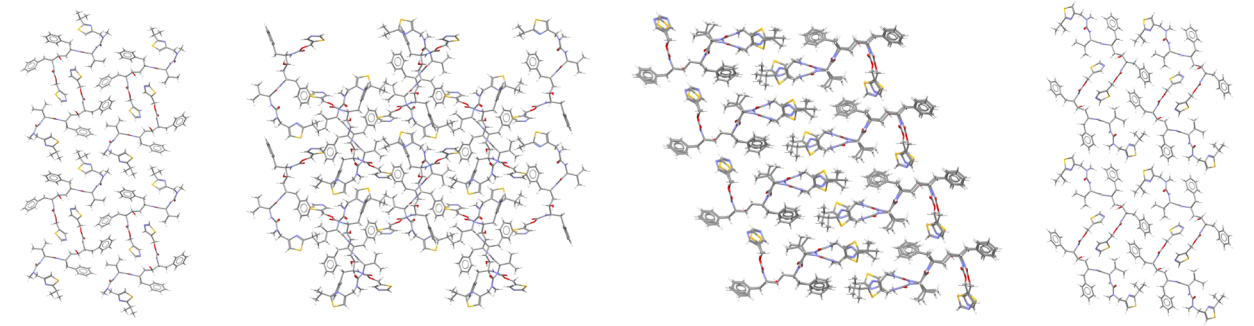

Figure 6. Molecular packing diagrams of Forms I, II, III, and IV (left to right).

https://doi.org/10.1021/acs.cgd.5c01571
Cryst. Growth Des. 2026, 26, 1386−1392

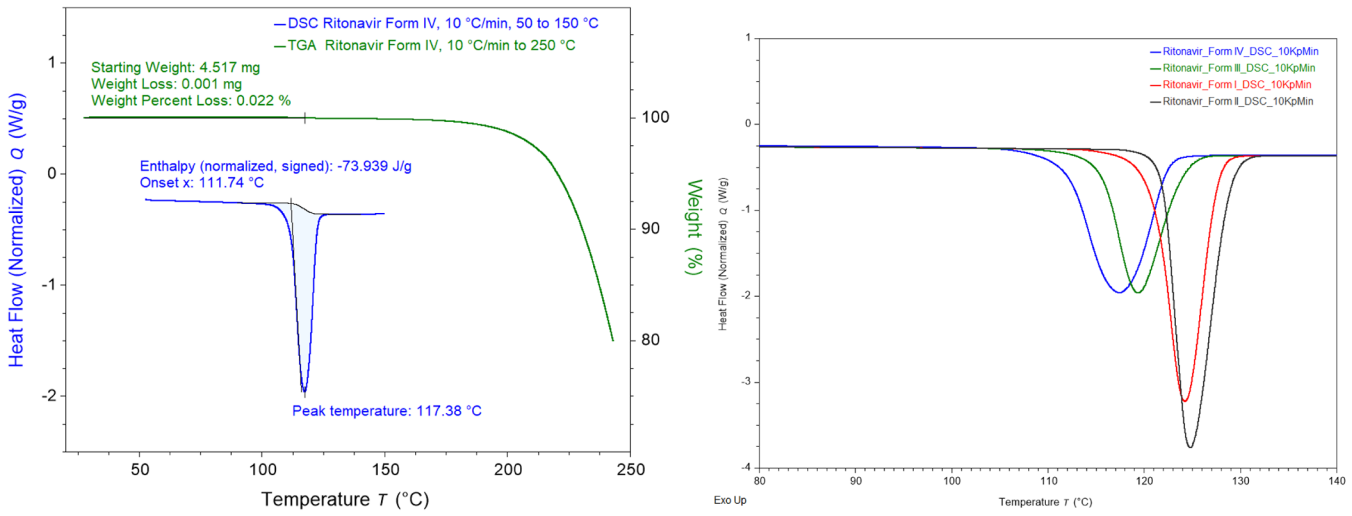

Figure 7. DSC and TGA thermograms of RTV Form IV (left) and a comparison of the DSC thermograms (right) for the RTV polymorphs, 10 °C/min.

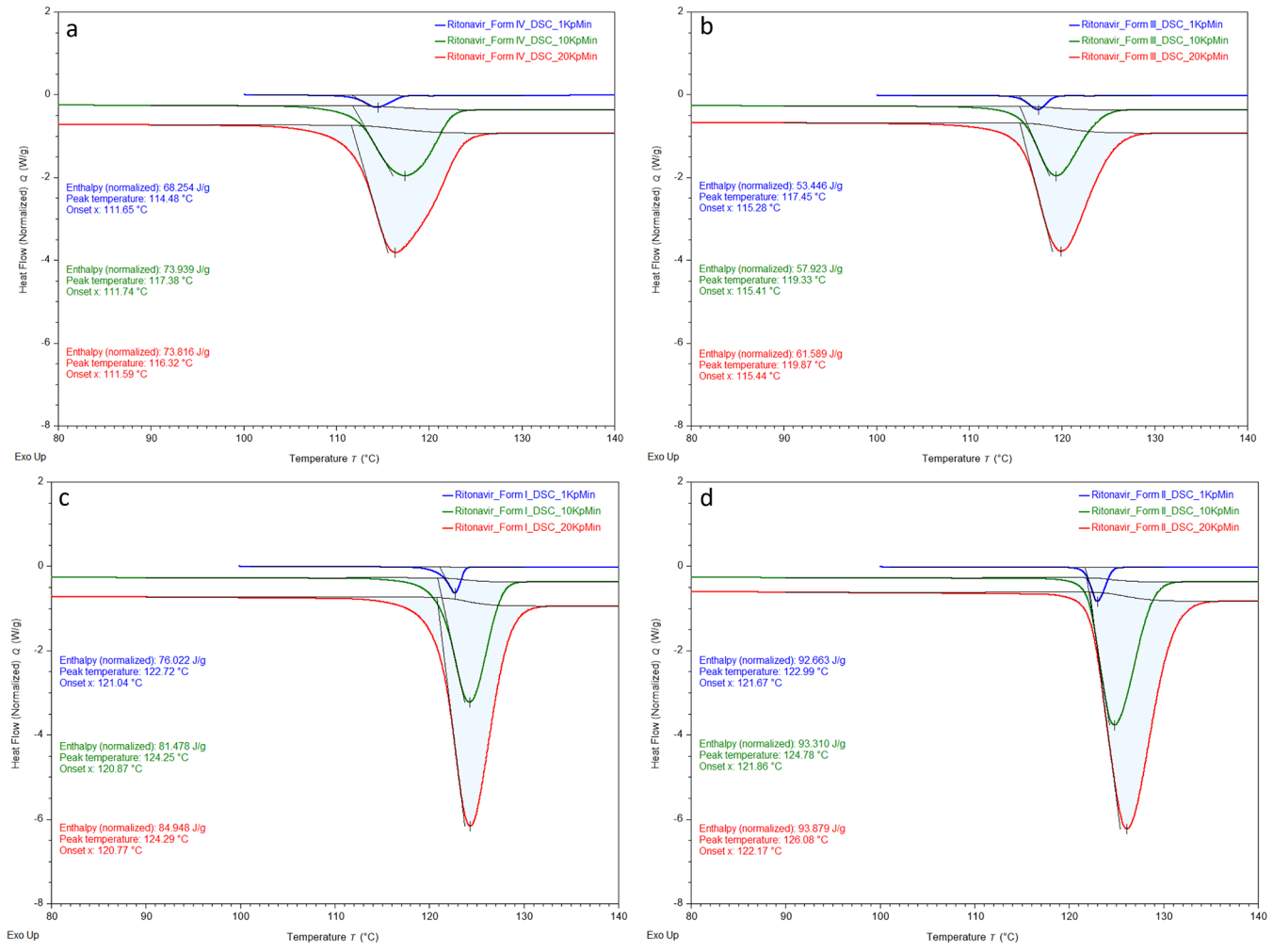

Figure 8. DSC thermograms obtained at 1 (blue), 10 (green), and 20 (red) °C/min for RTV Forms IV (a), III (b), I (c), and II (d).

The DSC thermograms and corresponding tabulated data in Table 2 were used to analyze the stability relationships of the four anhydrous polymorphs. Based on the data, RTV Forms IV and III were identified as enantiotropic. This means that at temperatures below their transition point (T_P), Form III is the least stable polymorph among the four. However, above T_P, the thermodynamic stability order reverses, and Form IV becomes the least stable.

The relative thermodynamic stability of the polymorphs at various temperatures can be qualitatively represented by a

https://doi.org/10.1021/acs.cgd.5c01571
Cryst. Growth Des. 2026, 26, 1386−1392

Table 2. Relevant Physical Properties of RTV Polymorphs and Derived Thermodynamic Relationships

			Relative Thermodynamic Relationship[a]		
	T_m (°C)	ΔHf(J/g)	Form I	Form II	Form III
Form I	120.9 ± 0.1	80.8 ± 4.5			
Form II	121.9 ± 0.3	93.3 ± 0.6	monotropic		
Form III	115.4 ± 0.1	57.7 ± 4.1	monotropic	monotropic	
Form IV	111.7 ± 0.1	71.8 ± 2.8	monotropic	monotropic	enantiotropic, $T_p \cong$ 99 °C[b,c]

[a]A virtual transition temperature above the melt implies monotropy. [b]Changes in heat capacity between transitions are estimated with a fixed ratio of 0.005/K, the upper bound proposed by Burger and Ramberger. [c]The transition temperature is estimated to be 97 °C when ignoring the contribution from changes in heat capacity, as in Behme's approach.

Gibbs free energy phase diagram, depicted in Figure 9. In this type of diagram, the free energy isobars for different phases are

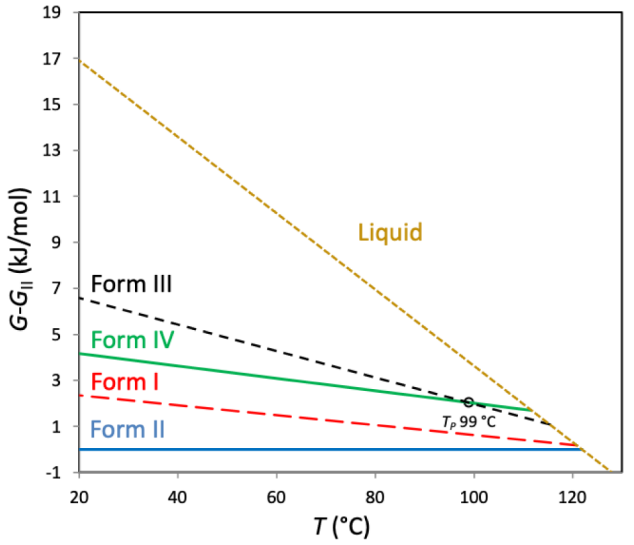

Figure 9. Gibbs free energy of RTV polymorphs relative to Form II.

plotted as a function of temperature. The simplified extrapolation of these relationships is possible because it is assumed that the Gibbs free energy difference between the polymorphs is approximately linear. The intersection of the free energy isobars for two polymorphs defines their phase transition temperature, while the intersection with that of the liquid defines its melting temperature (T_m).

Assuming the difference in heat capacity (ΔC_p) between the polymorphs is constant but nonzero, the T_P for RTV Forms IV and III is estimated to be approximately 99 °C.[24,25] If the ΔC_p contribution is ignored, the simplified equation for the free energy difference, $\Delta G_{liquid\text{-}crystal} = \Delta H_m (T_m - T)/ T_m$, yields a slightly lower estimate of around 97 °C for T_P.[26−29] Furthermore, the free energy phase diagram can be extrapolated to predict virtual phase transitions above the melting point for other polymorph pairs, which implies a monotropic relationship between them. This graphical representation is a powerful tool for understanding the complex thermodynamic relationships of Ritonavir polymorphs.

CONCLUSION

Decades after the RTV recall crisis demonstrated the importance of thermodynamic polymorph relationships, new polymorphs continue to be added. The crystal structure of the RTV Form IV has been determined through electron diffraction methods. Hydrogen bonding in the framework of Form IV is similar to that of Forms I and III. The relative thermodynamic stabilities of the four known anhydrous polymorphs were also established. Forms IV and III are enantiotropic with a conversion temperature of about 99 °C. All other forms are monotropic, with Form II as the most stable form.

ASSOCIATED CONTENT

Supporting Information

The Supporting Information is available free of charge at https://pubs.acs.org/doi/10.1021/acs.cgd.5c01571.

Supporting Information files have been submitted and include information regarding the electron diffraction. Tables for the data collection parameters, data quality statistics for individual data sets, and resolution for the merged data sets. Images of the crystallites and resulting diffraction images are also supplied (PDF)

Accession Codes

Deposition Number 2482055 contains the supplementary crystallographic data for this paper. These data can be obtained free of charge via the joint Cambridge Crystallographic Data Centre (CCDC) and Fachinformationszentrum Karlsruhe Access Structures service.

AUTHOR INFORMATION

Corresponding Author

Jared P. Smit − *Improved Pharma, LLC, West Lafayette, Indiana 47906, United States;* orcid.org/0000-0001-9474-4120; Email: jared.smit@improvedpharma.com

Authors

Stephan D. Parent − *Improved Pharma, LLC, West Lafayette, Indiana 47906, United States*

Dale K. Purcell − *Improved Pharma, LLC, West Lafayette, Indiana 47906, United States*

Pamela A. Smith − *Improved Pharma, LLC, West Lafayette, Indiana 47906, United States*

Pierre Le Maguerès − *Rigaku Americas, The Woodlands, Texas 77381, United States*

Haley C. Bauser − *Varda Space Industries, El Segundo, California 90245, United States*

Adrian Radocea − *Varda Space Industries, El Segundo, California 90245, United States;* orcid.org/0000-0002-4496-2573

Complete contact information is available at: https://pubs.acs.org/10.1021/acs.cgd.5c01571

https://doi.org/10.1021/acs.cgd.5c01571
Cryst. Growth Des. 2026, 26, 1386−1392

Notes

The authors declare the following competing financial interest(s): H.C. Bauser and A. Radocea are employees of Varda Space Industries and may own Varda Space Industries stock.

REFERENCES

(1) Lohani, S.; Grant, D. J. W. *Polymorphism: in the Pharmaceutical Industry.*; Hilfiker, R., Ed.; Wiley-VCH Verlag, 2006; pp. 21−42.
(2) Bernstein, J. *Polymorphism in Molecular Crystals*; Oxford University Press, 2020.
(3) Censi, R.; Di Martino, P. Polymorph Impact on the Bioavailability and Stability of Poorly Soluble Drugs. *Molecules* **2015**, *20* (10), 18759−18776.
(4) Jiménez Cruz, J. M.; Vlaar, C. P.; Stelzer, T.; López-Mejías, V. Polymorphism in Early Development: The Account of MBQ-167. *Int. J. Pharm.* **2021**, *608*, 121064.
(5) Bauer, J. F. Polymorphism-A Critical Consideration in Pharmaceutical Development, Manufacturing, and Stability. *J. Valid. Technol.* **2008**, *14* (5), 15−23.
(6) Henck, J.-O.; Kuhnert-Brandstatter, M. Demonstration of the Terms Enantiotropy and Monotropy in Polymorphism Research Exemplified by Flurbiprofen. *J. Pharm. Sci.* **1999**, *88*, 103−108.
(7) Burger, A.; Ramberger, R. On the Polymorphism of Pharmaceuticals and Other Molecular Crystals. I. *Mikrochim. Acta* **1979**, *72* (3−4), 259−271.
(8) Burger, A.; Ramberger, R. On the Polymorphism of Pharmaceuticals and Other Molecular Crystals. II. *Mikrochim. Acta* **1979**, *72* (3−4), 273−316.
(9) Chemburkar, S. R.; Bauer, J.; Deming, K.; Spiwek, H.; Patel, K.; Morris, J.; Henry, R.; Spanton, S.; Dziki, W.; Porter, W.; Quick, J.; Bauer, P.; Donaubauer, J.; Narayanan, B. A.; Soldani, M.; Riley, D.; McFarland, K. Dealing with the Impact of Ritonavir Polymorphs on the Late Stages of Bulk Drug Process Development. *Org. Process Res. Dev.* **2000**, *4*, 413−417.
(10) Morissette, S. L.; Soukasene, S.; Levinson, D.; Cima, M. J.; Almarsson, O. Elucidation of Crystal form Diversity of the HIV Protease Inhibitor Ritonavir by High-throughput Crystallization. *Proc. Natl. Acad. Sci. U. S. A.* **2003**, *100*, 2180−2184.
(11) Bauer, J.; Spanton, S.; Henry, R.; Quick, J.; Dziki, W.; Porter, W.; Morris, J. Ritonavir: An Extraordinary Example of Conformational Polymorphism. *Pharm. Res.* **2001**, *18*, 859−866.
(12) Kawakami, K.; Harada, T.; Miura, K.; Yoshihashi, Y.; Yonemochi, E.; Terada, K.; Moriyama, H. Relationship Between-Crystallization Tendencies During Cooling from Melt and Isothermal Storage: Toward a General Understanding of Physical Stability of Pharmaceutical Glasses. *Mol. Pharmaceutics* **2014**, *11*, 1835−1843.
(13) Yao, X.; Henry, R. F.; Zhang, G. G. Z. Ritonavir Form III: A New Polymorph After 24 Years. *J. Pharm. Sci.* **2023**, *112*, 237−242.
(14) Parent, S. D.; Smith, P. A.; Purell, D. K.; Smith, D. T.; Bogdanowich-Knipp, S. J.; Bhavsar, A. S.; Chan, L. R.; Croom, J. M.; Bauser, H. C.; McCalip, A.; Byrn, S. R.; et al. Ritonavir Form III: A Coincidental Concurrent Discovery. *Cryst. Gr. Des.* **2023**, *23*, 320−325.
(15) Parent, S.; Smith, P.; Bauser, H.; Radocea, A.Discovery and Characterization of a Transient Bis(dichloromethane) Solvate of Ritonavir: A Pathway to Metastable Form IV*Chem. Rxiv.***2024**
(16) Ito, S.; White, F. J.; Okunishi, E.; Aoyama, Y.; Yamano, A.; Sato, H.; Ferrara, J. D.; Jasnowski, M.; Meyer, M. Structure determination of small molecule compounds by an electron diffractometer for 3D ED/MicroED. *Cryst. Eng. Comm.* **2021**, *23*, 8622−8630.
(17) Dolomanov, O. V.; Bourhis, L. J.; Gildea, R. J.; Howard, J. A. K.; Puschmann, H. OLEX2: A complete structure solution, refinement, and analysis program. *J. Appl. Crystallogr.* **2009**, *42*, 339−341.
(18) Sheldrick, G. M. SHELXT − Integrated space-group and crystal-structure determination. *Acta Crystallogr.* **2015**, *A71*, 3−8.
(19) Sheldrick, G. M. Crystal structure refinement with SHELXL. *Acta Crystallogr.* **2015**, *C71*, 3−8.
(20) Li, S.; Liu, B.; Chen, Z.; Ou, X.; Rong, H.; Lu, M. Ritonavir Revisited: Melt Crystallization Can Easily Find the Late-Appearing Polymorph II and Unexpectedly Discover a New Polymorph III. *Mol. Pharmaceutics.* **2023**, *20*, 3854−3863.
(21) Gaisford, S.; Buanz, A. B. M. Pharmaceutical Physical Form Characterization with Fast DSC Heating Rates. *J. Therm. Anal. Calorim.* **2011**, *106* (1), 221−226.
(22) Saunier, J.; Herry, J.-M.; Yagoubi, N.; Marlière, C. Exploring Complex Transitions between Polymorphs on a Small Scale by Coupling AFM, FTIR and DSC: The Case of Irganox 1076® Antioxidant. *RSC Advances* **2017**, *7* (7), 3804−3818.
(23) Wang, G.; Harrison, I. R. Polymer Melting: Heating Rate Effects on DSC Melting Peaks. *Thermochim. Acta* **1994**, *231*, 203−213.
(24) Grunenberg, A.; Henck, J.-O.; Siesler, H. W. Theoretical Derivation and Practical Application of Energy/Temperature Diagrams as an Instrument in Preformulation Studies of Polymorphic Drug Substances. *Int. J. Pharm.* **1996**, *129* (1−2), 147−158.
(25) Yu, L. Inferring Thermodynamic Stability Relationship of Polymorphs from Melting Data. *J. Pharm. Sci.* **1995**, *84* (8), 966−974.
(26) Cassel, R. B.; Behme, R. A DSC Method to Determine the Relative Stability of Pharmaceutical Polymorphs. *Am. Lab.* **2004**, *36*, 26−29 + 10.
(27) Behme, R. J.; Brooke, D. Heat of Fusion Measurement of a Low Melting Polymorph of Carbamazepine That Undergoes Multiple-Phase Changes during Differential Scanning Calorimetry Analysis. *J. Pharm. Sci.* **1991**, *80* (10), 986−990.
(28) Pudipeddi, M.; Serajuddin, A. T. M. Trends in Solubility of Polymorphs. *J. Pharm. Sci.* **2005**, *94* (5), 929−939.
(29) Hoffman, J. D. Thermodynamic Driving Force in Nucleation and Growth Processes. *J. Chem. Phys.* **1958**, *29* (5), 1192−1193.

https://doi.org/10.1021/acs.cgd.5c01571
Cryst. Growth Des. 2026, 26, 1386−1392